



# Effects of heteroaggregation with metal oxides and clays on tetracycline adsorption by graphene oxide

Meifang Li<sup>a,b</sup>, Yunguo Liu<sup>a,b,\*</sup>, Chunping Yang<sup>c,\*\*</sup>, Shaobo Liu<sup>d</sup>, Xiaofei Tan<sup>a,b</sup>, Yuan He<sup>a,b</sup>, Ni Liu<sup>a,b</sup>, Lu Zhou<sup>e</sup>, Xiaoxi Cai<sup>f</sup>, Jun Wen<sup>g</sup>

<sup>a</sup> College of Environmental Science and Engineering, Hunan University, Changsha 410082, PR China

<sup>b</sup> Key Laboratory of Environmental Biology and Pollution Control, Ministry of Education, Hunan University, Changsha 410082, PR China

<sup>c</sup> Guangdong Provincial Key Laboratory of Petrochemical Pollution Process and Control, Guangdong University of Petrochemical Technology, Maoming 525000, PR China

<sup>d</sup> School of Architecture and Art, Central South University, Changsha 410083, PR China

<sup>e</sup> School of Hydraulic Engineering, Changsha University of Science and Technology, Changsha 410114, PR China

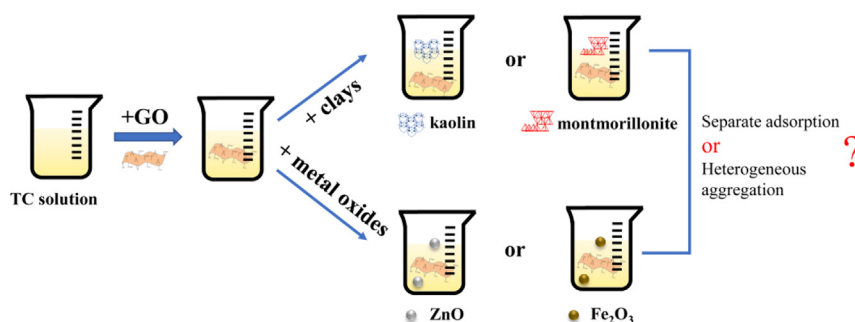
<sup>f</sup> College of Art and Design, Hunan First Normal University, Changsha 410205, PR China

<sup>g</sup> College of Agriculture, Guangxi University, Nanning 530005, PR China

## HIGHLIGHTS

- The presence of m-NPs increased the adsorption equilibrium time of TC onto GO.
- m-NPs promoted TC adsorption due to the adsorption of TC onto m-NPs.
- The introduction of m-NPs led to the increase of TC adsorption on GO at various pH.
- m-NPs/GO had greatest promoting effect on TC removal among five m-NPs/adsorbents.
- The heteroaggregation mechanism was studied by TEM images and DLVO calculation.

## GRAPHICAL ABSTRACT



## ARTICLE INFO

### Article history:

Received 2 December 2019

Received in revised form 18 January 2020

Accepted 11 February 2020

Available online xxxx

Editor: Baoliang Chen

### Keywords:

Graphene oxide  
Tetracycline  
Metal oxides  
Clays  
Adsorption  
DLVO analysis

## ABSTRACT

Multiple nanoparticles (NPs) often coexist in water with contaminants, which inevitably affect the fate and transport of coexisted contaminants and other types of nanoparticles in actual water. This research was devoted to examine the adsorption of tetracycline (TC) on graphene oxide (GO) in the presence of different amounts of model engineered and natural NPs (m-NPs), including metal oxides (ZnO and Fe<sub>2</sub>O<sub>3</sub>), clays (kaolin and montmorillonite). The experimental results proved that the existence of m-NPs greatly enhanced the TC adsorption onto GO except for that at Fe<sub>2</sub>O<sub>3</sub>/GO = 10:1 and lengthened the adsorption equilibrium time. The enhanced adsorption amount of TC with increasing m-NPs/GO ratio was primarily due to the adsorption of TC onto m-NPs. In contrast, the slightly inhibitory effects by 10:1 Fe<sub>2</sub>O<sub>3</sub>/GO could be attributed to the blockage effect on GO surface by a small amount of Fe<sub>2</sub>O<sub>3</sub>. Compared with five m-NPs/adsorbents, m-NPs/GO had the greatest promoting efficiency on TC removal. Moreover, the heteroaggregation of GO with different m-NPs was studied in aqueous phase by microscopic, spectroscopic, and computational methods. Analysis showed that the electrostatic attraction between negatively charged GO and positively charged ZnO were likely to first heteroaggregate in binary systems of GO and ZnO, while GO were prone to homoaggregate owing to electrostatic repulsion with the same negatively charged montmorillonite (or kaolin). Besides, Fe<sub>2</sub>O<sub>3</sub> tended to first homoaggregate and then heteroaggregate

\* Correspondence to: Y. Liu, College of Environmental Science and Engineering, Hunan University, Changsha 410082, PR China.

\*\* Corresponding author.

E-mail addresses: [liuyunguo\\_hnu@163.com](mailto:liuyunguo_hnu@163.com) (Y. Liu), [yangc@hnu.edu.cn](mailto:yangc@hnu.edu.cn) (C. Yang).

with GO. In summary, this report elucidated complex interactions between GO and m-NPs, which was crucial to fundamentally understand towards a predictive framework for describing the fate and migration of GO and m-NPs in actual water.

© 2020 Elsevier B.V. All rights reserved.

## 1. Introduction

Nanoparticles (NPs), including natural and engineered nanoparticles, have been widely used in human life, such as pharmaceuticals, cosmetics, building materials, and electronic devices fields (Andre et al., 2006). At present, engineered nanoparticles are mainly divided into the following categories: carbonaceous nanoparticles (e.g. graphene and biochar), metal oxides (e.g. Fe<sub>2</sub>O<sub>3</sub> and ZnO), zerovalent metals (e.g. silver), semiconductors (e.g. SiO<sub>2</sub>), and nanopolymers (e.g. dendrimers) (Bhatt and Tripathi, 2011). Among them, carbonaceous nanoparticles and metal oxides, due to their unique physicochemical properties, occupy the larger market share in the manufacturing and application of NPs (Shi et al., 2017). Besides, clays (e.g. kaolin, montmorillonite) as a kind of natural nanoparticles have wide applications in cosmetics, therapeutic and medicine, as well as wine clarification in the food industry. Moreover, clay minerals are also used for environmental protection and remediation (Awad et al., 2019; Ji and Pei, 2019), making them ubiquitous in the natural environment.

Graphene is one kind of typical carbonaceous nanoparticles, which is composed of honeycomb structure of conjugated carbon atoms with sp<sup>2</sup>-hybridized single layer (Yu et al., 2016). It is a basic unit for many carbonaceous materials, such as fullerenes, nanotubes, and three-dimensional graphite (Jiang et al., 2018a). Since its discovery in 2004, due to its special structure, high specific surface area, and excellent mechanical, electrical, thermal and optical properties, graphene is regarded as ideal candidates for many organic pollutants adsorption (Wang et al., 2013; Yusuf et al., 2015; Zhang et al., 2019). Large scale production of graphene industry is expected to grow continuously in the next ten years (Zhou et al., 2015). However, mass production will unavoidably be released into the environment, thus bring serious hazards to human health and ecological systems. Tetracyclines, as a class of commonly used antibiotics, are frequently detected in ground water, surface water, and even drinking water (Li et al., 2019), which poses a threat to the aquatic environment, including the toxicity to aquatic organisms and the dissemination of antibiotic resistance genes among microorganisms. Some side effects of graphene could be increased because of the adsorption of tetracyclines pollutants, and the fate and migration of tetracyclines might also be changed in the environment. Thus, an in-depth understanding of the adsorption behavior and environmental risks of graphene nanomaterials in adsorbing tetracyclines contaminants is essential.

In natural water systems, multiple NPs often coexist in wastewater. NPs can not only react with pollutants, but also it can react with other types of NPs. These reactions can occur simultaneously or continuously, and will be the crucial factor determining the fate, transport, and toxicity of contaminants and NPs (Sun et al., 2015). Sorption of various organic contaminants (e.g. antibiotics, dyes, and endocrine disruptor compounds) by single carbonaceous nanoparticles at a time has been extensively studied (Gao et al., 2012; Lin et al., 2013; Zhang et al., 2011; Zhou et al., 2017). Until now, lots of researches had been reported that graphene nanomaterials possessed good adsorbability to multiple antibiotics contaminants owing to their huge specific surface area and strong  $\pi$ - $\pi$  interactions (Chen et al., 2015; Ghadim et al., 2013; Liu et al., 2016; Rashidi Nodeh and Sereshti, 2016). However, little attention has been placed on study the effects of various NPs on antibiotics adsorption by graphene nanomaterials. In fact, pollutants adsorption by multiple NPs can occur inevitably once they are released into water environment. In addition, because of the ubiquity of multiple NPs in

natural waters, heterogeneous adsorption may be more important than homogeneous adsorption in determining the direction and migration of contaminants in aqueous solution (Ki-Tae et al., 2009). When graphene nanomaterials are released into natural waters, the aggregation or interaction of these nanomaterials with other NPs is inevitable, which will affect their adsorption behaviors (Duan et al., 2019). Accordingly, it is very valuable to investigate the adsorption behavior of adsorbent in the presence of natural aquatic particles, which is of great significance to predict its application prospects in practical use.

As reported, the presence of metal oxides (SiO<sub>2</sub> and Al<sub>2</sub>O<sub>3</sub>) had two main impacts on 17 $\beta$ -estradiol (E2) uptake by graphene oxide (GO), namely heteroaggregation and homoaggregation (Jiang et al., 2018b). Moreover, the size-dependent effect of SiO<sub>2</sub> and Al<sub>2</sub>O<sub>3</sub> on the sorption of sulfamethoxazole by carbon nanotubes (CNTs) was explored (Chen et al., 2017). However, as we know, few studies have been carried out to investigate the influence of various NPs on antibiotics removal by different adsorbents, such as graphenes, CNTs, biochar (BC), and activated carbon (ACs). For this study, GO was selected as adsorbents, metal oxides (ZnO and Fe<sub>2</sub>O<sub>3</sub>) and clays (kaolin and montmorillonite) nanoparticles were selected as model engineered and natural NPs (m-NPs). Tetracycline (TC) was chosen as a target antibiotic pollutant. Adsorption kinetics and isotherms on the TC adsorption by GO were examined with the coexistence of m-NPs, and the impacts of pH and different amounts of m-NPs on these processes were discussed. Besides, although CNTs, BC, and ACs have been used to explore the adsorption properties of TC, the influence of m-NPs on the adsorption of TC by various carbonaceous materials has not been paid enough attention. Therefore, the specific purpose of this study was to compare the adsorption characteristics of graphene nanomaterials with other common carbonaceous materials in the absence and presence of m-NPs, including multi-walled carbon nanotube (MWCNT), BC, powdered activated carbon (PAC), and granular activate carbon (GAC). Finally, based on zeta potentials, transmission electron microscopy (TEM), and DLVO calculation, the potential influencing mechanisms were clarified.

## 2. Materials and methods

### 2.1. Materials

GO was prepared according to the modified Hummers method (Li et al., 2017b). The specific preparation methods of GO were described in the Supplementary Materials. The MWCNT was purchased from Chengdu Organic Chemicals Co., Ltd., China. Rice straw was provided by a farm in Yiyang, Hunan province, China. BC was prepared by pyrolysis of straw at 600 °C and the detailed synthesis process was described in the Supplementary Materials. ACs (PAC and GAC) were obtained from Sinopharm Chemical Reagent Co., Ltd., China. The obtained GO, MWCNT, BC, and PAC could be used directly, but the GAC needed to be crushed to 150–225  $\mu$ m size before use.

Tetracycline hydrochloride was provided by Hefei Bomei Biotechnology Co., Ltd., China. Fe<sub>2</sub>O<sub>3</sub> m-NPs (purity  $\geq$ 99%), ZnO m-NPs (purity  $\geq$ 99%), kaolin, NaOH, HCl, and other chemical reagents were obtained from Sinopharm Chemical Reagent Co., Ltd., China. Montmorillonite was purchased from Shanghai Aladdin Bio-Chem Technology Co., Ltd., China. All chemicals were of analytical grade during the entire experiment process and prepared with deionized water (18.25  $\Omega$ /cm).

## 2.2. Characterizations

Brunauer-Emmett-Teller (BET) surface area and pore volume of the samples were characterized by multipoint  $N_2$  adsorption-desorption at 77 K using a Quadrasorb EVO instrument (Quantachrome, USA). The compositions of surface elements and functional groups of GO were determined by X-ray photoelectron spectroscopy (XPS) (Thermo Fisher, USA) and Fourier transform infrared spectrum (FT-IR) (Shimadzu, Japan). The surface structure and morphology were performed by a transmission electron microscopy (TEM) (Tecnai G2 F20, USA). The phase structure of m-NPs was investigated by a Bruker D8-Advance X-ray diffractometer (XRD) (Bruker, German). The zeta potentials and particle sizes of samples were determined by dynamic light scattering (DLS) measurements using a zeta potential meter (Zetasizer Nano-ZS90, Malvern).

## 2.3. Adsorption experiments

Batch experiments were carried out in 25 mL 0.01 mol/L NaCl background electrolyte at 25 °C. In the study of adsorption kinetics, various m-NPs/GO ratios (0:1, 10:1, 50:1 and 100:1) were obtained by adding specific amounts of m-NPs into the suspension of GO. The suspension was mixed in a rotary shaker for 30 min at 180 rpm, and then TC was added into the solution at initial concentration of 50 mg/L. The samples were analyzed at different time intervals from 0 to 1440 min. Isotherm experiments were performed at the initial concentrations of TC from 50 to 300 mg/L. To evaluate the influence of pH, the acidity and alkalinity of different solutions (3–11) were adjusted by negligible volume of HCl or NaOH at 50 mg/L TC. The comparison of TC adsorption by MWCNT, BC, PAC, and GAC in different amounts of m-NPs were conducted by adding 0.005 g adsorbent at 150 rpm for 24 h. The experimental data were reported as the average of three duplicate experiments.

The supernatant was filtered by 0.45  $\mu\text{m}$  water system microporous membranes. Residual TC concentrations were determined with an UV-Vis spectrophotometer (UV-2550, SHI-MADZU, Japan) at a wavelength of 357 nm (Li et al., 2017a). The amount of TC adsorbed was calculated based on the following equation:

$$q_e = \frac{(C_0 - C_e)V}{m} \quad (1)$$

where  $C_0$  and  $C_e$  represent the TC initial and equilibrium concentrations, respectively (mg/L);  $V$  stands for the solution volume (L) and  $m$  is the adsorbent mass (g).

## 3. Results and discussion

### 3.1. Characterization of adsorbents

FT-IR spectrum is conducted to investigate the bonding links of GO. In the FT-IR spectrum (Fig. 1a), some characteristic peaks of oxidized

groups were detected at  $3415\text{ cm}^{-1}$  (O—H stretching vibrations), at  $1723\text{ cm}^{-1}$  (C=O stretching vibrations), at  $1391\text{ cm}^{-1}$  (C—O stretching vibrations), and at  $1079\text{ cm}^{-1}$  (C—O stretching vibrations) (Yang et al., 2010; Yao et al., 2012). The peak around  $1628\text{ cm}^{-1}$  corresponded to the skeletal vibration of C=C bond (Yin et al., 2018; Zhu et al., 2018). Furthermore, the chemical composition and atomic concentrations of GO were evaluated by XPS (Geng et al., 2009). XPS further confirmed that the existence of oxygen and the oxygen percentage was around 32.7% and carbon percentage was 65.8% in mass. The C1s spectrum of GO (as shown in Fig. 1b) contained four major peaks after deconvolution at 284.24, 285.04, 286.86, and 288.54 eV, which were assigned as the carbon in C=C, C—O, C=O, and O—C=O, respectively (Liu et al., 2019b; Wang et al., 2014).

The surface area was found to be 248.2, 99.8, 10.1, 4.2, and 5.2  $\text{m}^2/\text{g}$  for GO, montmorillonite, kaolin, ZnO and  $\text{Fe}_2\text{O}_3$ , respectively. Total pore volume followed the order of montmorillonite ( $0.162\text{ cm}^3/\text{g}$ ) > GO ( $0.159\text{ cm}^3/\text{g}$ ) > kaolin ( $0.056\text{ cm}^3/\text{g}$ ) > ZnO ( $0.020\text{ cm}^3/\text{g}$ ) >  $\text{Fe}_2\text{O}_3$  ( $0.019\text{ cm}^3/\text{g}$ ) m-NPs. There was little difference in total pore volume between ZnO and  $\text{Fe}_2\text{O}_3$ .

XRD is an important tool for examining the crystal structure of m-NPs. The XRD pattern of m-NPs is performed in Fig. 1c. For  $\text{Fe}_2\text{O}_3$ , the analysis revealed eleven strong peak at  $2\theta = 24.2^\circ, 33.2^\circ, 35.7^\circ, 41.0^\circ, 49.6^\circ, 54.2^\circ, 57.7^\circ, 62.5^\circ, 64.1^\circ, 72.1^\circ,$  and  $75.6^\circ$  corresponding to the (012), (104), (110), (113), (024), (116), (018), (214), (300), (1010), and (220) planes from the cubic structure of  $\gamma\text{-Fe}_2\text{O}_3$  (JCPDS, No. 04-0755) (Abdelrahman et al., 2019; Asfaram et al., 2016). For ZnO, nine strong diffraction peak at  $2\theta = 31.9^\circ, 34.5^\circ, 36.4^\circ, 47.7^\circ, 56.7^\circ, 63.0^\circ, 66.4^\circ, 68.0^\circ,$  and  $69.2^\circ$  could be indexed to (100), (002), (101), (102), (110), (103), (200), (112), and (201) crystal planes, respectively, which matched well with the indexed peaks of pure hexagonal ZnO (JCPDS No. 36-1451) (Chen et al., 2013; Ghaedi et al., 2014). XRD pattern of montmorillonite showed the characteristic peak at  $2\theta = 5.84^\circ$  corresponding to the (001) plane, which was attributed to the interlayer structure (Liu et al., 2019a). Two apparent peaks appeared at  $2\theta = 12.4^\circ$  and  $24.5^\circ$  corresponded to the (001) and (002) planes of kaolin, which were typical for kaolin group minerals. Another diffraction peak of kaolin at  $2\theta = 26.2^\circ$  corresponded to the plane (011) of  $\alpha\text{-quartz}$  (JCPDS card number 89-8937), which suggested the presence of quartz, and quartz together with kaolinite was the main minerals of the kaolin sample (Olusegun et al., 2018; Shaban et al., 2017).

### 3.2. Effects of contact time

The adsorption kinetics of TC on GO in the absence and existence of m-NPs are presented in Fig. 2. TC adsorbed amount enhanced with increasing reaction time and reached equilibrium under approximately 240 min in the GO-TC system. In comparison, the equilibrium time was much slower in the heterogeneous systems of m-NPs and GO. The

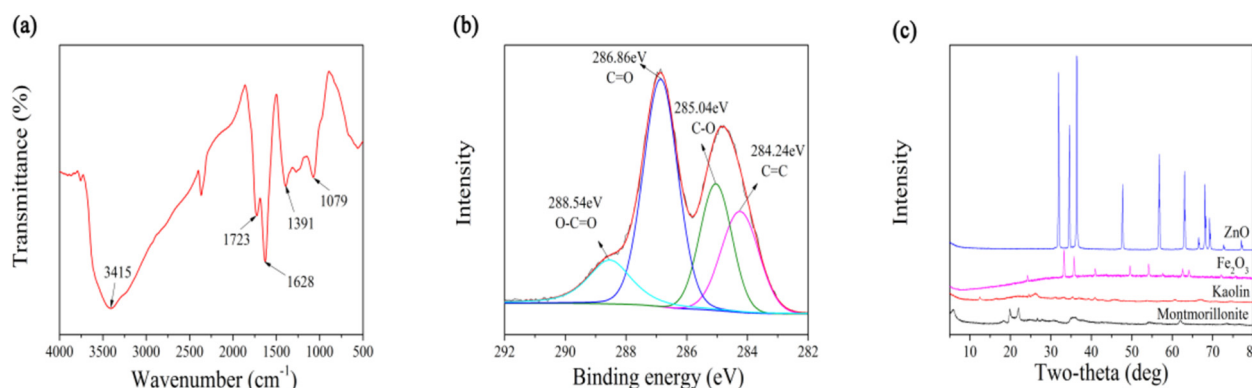
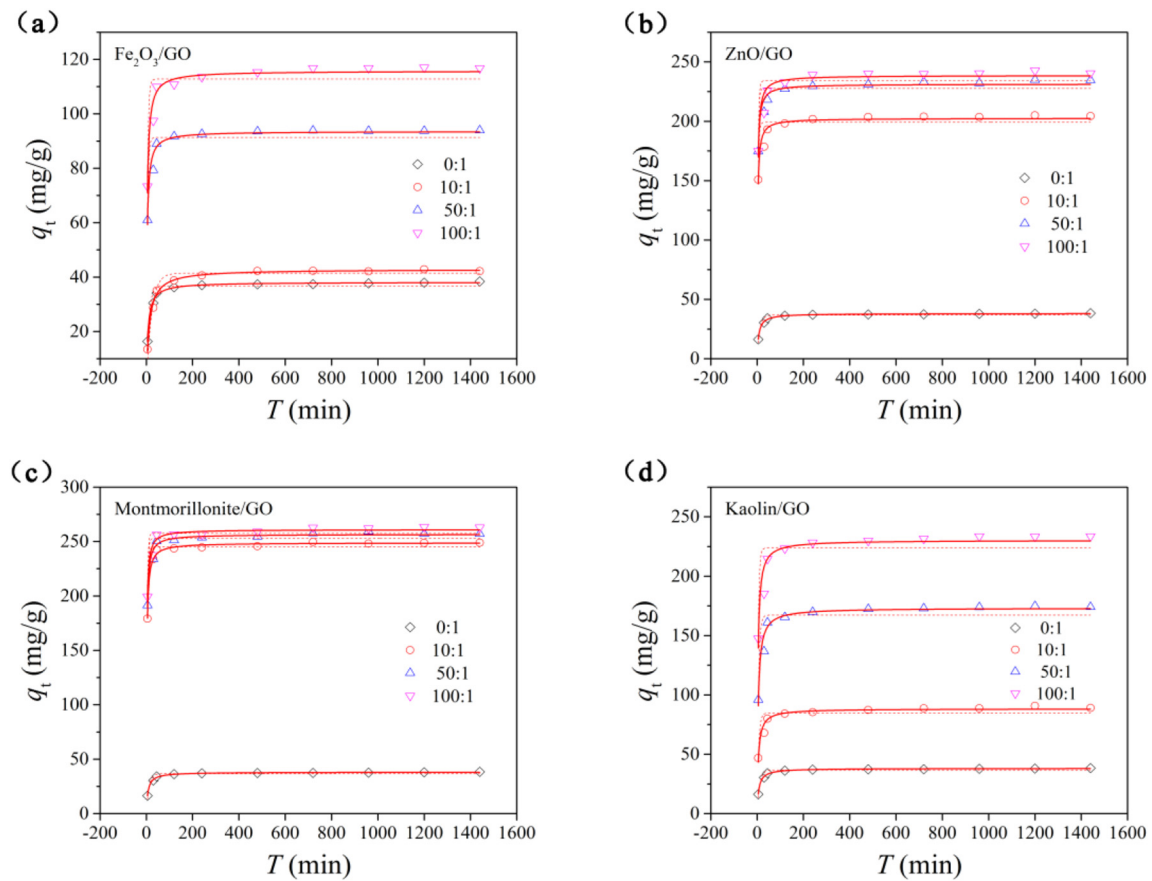


Fig. 1. FT-IR (a) and C 1s XPS (b) spectrum of GO; XRD patterns of montmorillonite, kaolin, ZnO, and  $\text{Fe}_2\text{O}_3$  (c).



**Fig. 2.** Adsorption kinetics curves of TC onto GO under different m-NPs/GO ratios (the solid lines and dotted lines are the pseudo-second-order model and the pseudo-first-order model simulation, respectively).  $C_{0(TC)} = 50$  mg/L,  $T = 25$  °C, pH = 7.0,  $I = 0.01$  M NaCl.

results showed that the existence of m-NPs slowed down the adsorption of TC onto GO.

The pseudo-first order (PFO) and pseudo-second order (PSO) models were employed to fit the adsorption kinetics data. The nonlinear fitting results of PFO and PSO models are reflected in Fig. 2 and Table 1. In comparison with the pseudo-first order model ( $R^2 = 0.698\text{--}0.948$ ), the pseudo-second order model fitted the experimental data better, as evidenced by the relatively higher  $R^2$  values (0.904–0.995) and closer values between the experimental values ( $q_{e,exp}$ ) and the calculated equilibrium adsorption capacity ( $q_{e,cal}$ ). Therefore, the chemisorption might be the rate-limiting step in the TC adsorption process and the

adsorption rate was proportional to the number of active sites on the GO surface. As displayed in Table 1, the calculated kinetic rate constants,  $k_2$ , all decrease with the addition of various m-NPs, especially, decrease with increasing m-NPs/GO ratio from 0:1 to 100:1 for kaolin and ZnO. It indicated that the adsorption sites of GO might be occupied or/and blocked by the m-NPs and the occupying or/and blocking effect was more significant with increasing ZnO/GO and kaolin/GO ratios (Sun et al., 2015). Differently,  $k_2$  slightly increased with increasing montmorillonite/GO and  $Fe_2O_3$ /GO ratios except for that at  $Fe_2O_3$ /GO = 50:1. The different effects of montmorillonite and  $Fe_2O_3$  on TC might be caused by the different properties of these substrates (Chen et al., 2017).

**Table 1**  
The parameters of TC adsorption kinetic on GO in the existence of m-NPs.

Adsorbents	$q_{e,exp}$ (mg/g)	Pseudo-first-order model			Pseudo-second-order model			
		$k_1$ (1/min)	$q_{e,1}$ (mg/g)	$R^2$	$k_2$ (g/mg min)	$q_{e,2}$ (mg/g)	$R^2$	
$Fe_2O_3$ /GO	0:1	37.95	0.0913	36.79	0.906	0.0039	38.14	0.995
	10:1	42.34	0.0444	41.48	0.940	0.0019	42.88	0.991
	50:1	93.88	0.2181	91.34	0.802	0.0037	93.56	0.954
	100:1	116.82	0.2075	112.77	0.795	0.0027	115.74	0.951
ZnO/GO	0:1	37.95	0.0913	36.79	0.906	0.0039	38.14	0.995
	10:1	204.30	0.2826	199.13	0.754	0.0026	202.48	0.923
	50:1	234.71	0.2917	227.69	0.770	0.0025	231.28	0.935
	100:1	240.45	0.2741	234.29	0.722	0.0021	238.59	0.906
Montmorillonite/GO	0:1	37.95	0.0913	36.79	0.906	0.0039	38.14	0.995
	10:1	248.96	0.2623	245.11	0.948	0.0021	248.80	0.992
	50:1	257.15	0.2830	252.84	0.863	0.0022	256.58	0.969
	100:1	262.82	0.2979	257.48	0.836	0.0024	261.02	0.951
Kaolin/GO	0:1	37.95	0.0913	36.79	0.906	0.0039	38.14	0.995
	10:1	88.96	0.1475	84.95	0.754	0.0022	88.34	0.947
	50:1	174.09	0.1619	167.20	0.779	0.0013	173.16	0.952
	100:1	233.55	0.2119	223.81	0.698	0.0013	230.22	0.904

Although the above kinetic models deduced the possible adsorption behavior in the TC uptake onto GO, they were not able to determine the actual transfer steps. The intra-particle diffusion model was applied to further analyze the rate-limiting step (Fig. 3). As illustrated in Fig. 3, the plot of  $q_t$  versus  $t^{0.5}$  for the TC adsorption exhibit the two-stage linearity, suggesting the adsorption process includes multiple steps. The first stage of this reaction had enough effective adsorption sites on the GO surface with high adsorption rate, indicated that the diffusion of TC molecule occurred from the mixed solution to the external surface of GO (film diffusion). The second stage represented the gradual adsorption stage due to the TC molecules suffered the hindrance when TC transferred to inner pores (intra-particle diffusion) (Hu et al., 2015; Kenawy et al., 2019). These results confirmed that the adsorption might be a complicated combination of involving both film diffusion and intra-particle diffusion. The kinetic parameters of TC intra-particle diffusion in the heterogeneous system of m-NPs/GO are exhibited in Table 2. The values of intercept  $L$  reflected the information about the boundary layer effect (Shi et al., 2017). As exhibited by Table 2, almost all increased  $L$  values in Stage I and II reveal a positive contribution of m-NPs to the initial film diffusion and intra-particle diffusion of TC onto GO, thus promoting TC adsorption. According to the change of  $L$  values, the addition of m-NPs played a greater role in the Stage II than Stage I.

### 3.3. Adsorption isotherms

Fig. 4 displays the adsorption isotherms of TC adsorption on GO and their mixtures with m-NPs at 298 K. The fitting adsorption isotherm data by the Langmuir and Freundlich models are tabulated in Table 3. By comparing the values of  $R^2$ , RMSE, and  $\chi^2$ , it was obvious that the

**Table 2**

TC adsorption parameters calculated by intra-particle diffusion model in the existence of m-NPs.

Adsorbents		Stage I			Stage II		
		$k_{d1}$ (mg/g min <sup>0.5</sup> )	$L_1$ (mg/g)	$R^2$	$k_{d2}$ (mg/g min <sup>0.5</sup> )	$L_2$ (mg/g)	$R^2$
Fe <sub>2</sub> O <sub>3</sub> /GO	0:1	4.0433	7.54	0.990	0.1043	34.62	0.750
	10:1	4.8061	2.63	0.999	0.1983	36.18	0.668
	50:1	6.1578	46.85	0.988	0.1265	89.86	0.667
	100:1	8.0387	54.92	0.990	0.2363	109.14	0.863
ZnO/GO	0:1	4.0433	7.54	0.990	0.1043	34.62	0.750
	10:1	9.2954	129.48	0.988	0.3089	194.52	0.708
	50:1	9.7969	153.20	0.997	0.4245	220.31	0.739
	100:1	11.1099	149.29	0.978	0.4032	228.31	0.639
Montmorillonite/GO	0:1	4.0433	7.54	0.990	0.1043	34.62	0.750
	10:1	14.7012	147.81	0.958	0.2218	241.35	0.852
	50:1	13.1693	162.01	0.999	0.2554	249.26	0.786
	100:1	12.4720	171.09	0.993	0.2665	253.79	0.887
Kaolin/GO	0:1	4.0433	7.54	0.990	0.1043	34.62	0.750
	10:1	7.2416	30.13	0.981	0.2790	80.28	0.834
	50:1	14.1545	63.16	0.976	0.3978	161.38	0.815
	100:1	14.3441	113.48	0.937	0.5229	216.34	0.776

adsorption isotherms of TC were simulated by the Freundlich model better than the Langmuir model even in the existence of m-NPs, suggesting the TC sorption on GO was mainly controlled by the heterogeneous chemisorption (Razmi et al., 2019). The presence of different amounts of m-NPs promoted the TC adsorption to GO with increasing TC concentration except for that at Fe<sub>2</sub>O<sub>3</sub>/GO = 10:1. Clearly, the  $K_f$  values of montmorillonite/GO, ZnO/GO, kaolin/GO and Fe<sub>2</sub>O<sub>3</sub>/GO increased from 1.33 to 1012.54, 255.67, 187.56, 56.82 (mg/g)/(mg/L)<sup>N</sup>, respectively,

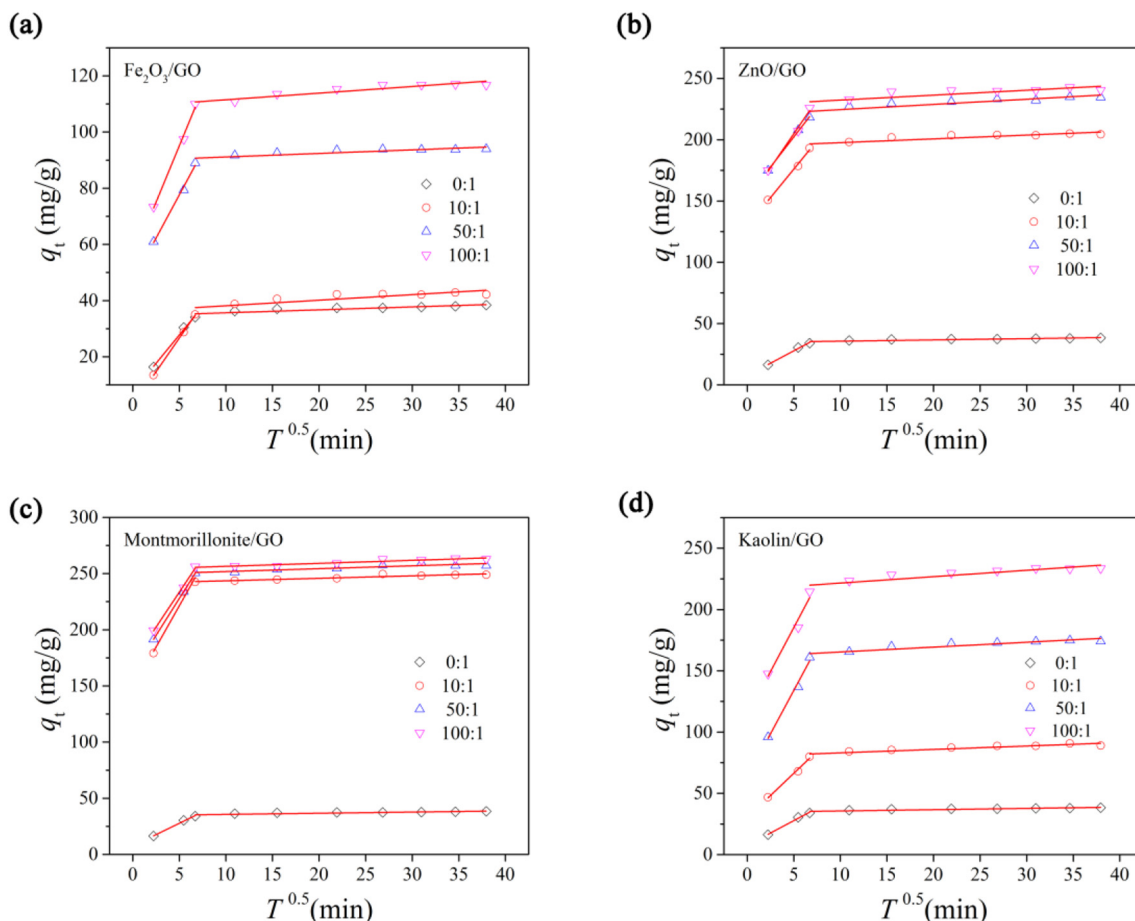


**Fig. 3.** Intra-particle diffusion model of TC adsorption onto GO in the existence of m-NPs.  $C_{0(TC)} = 50$  mg/L,  $T = 25$  °C,  $pH = 7.0$ ,  $I = 0.01$  M NaCl.

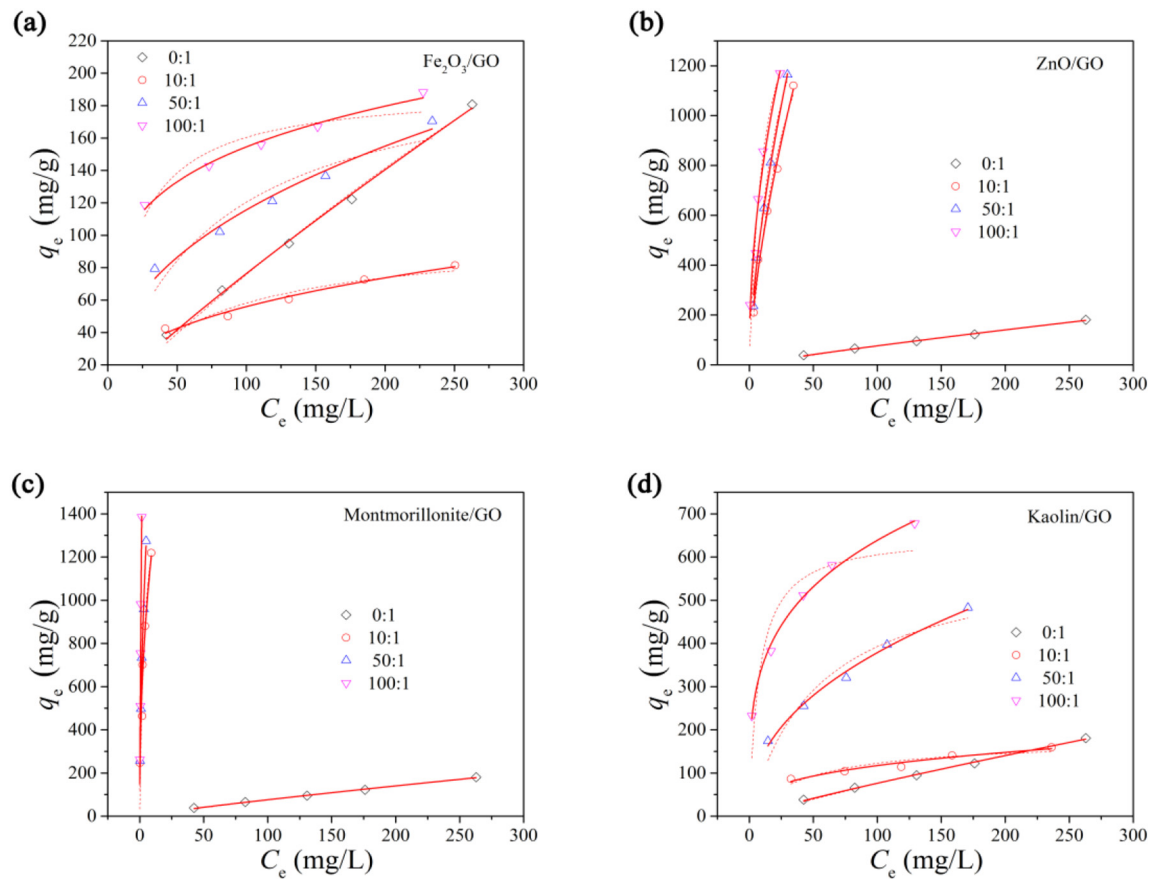


**Fig. 4.** Isotherms of TC adsorption onto GO under different m-NPs/GO ratios (the solid lines and dotted lines are the Freundlich model and Langmuir model simulation, respectively).  $T = 25\text{ }^{\circ}\text{C}$ ,  $\text{pH} = 7.0$ ,  $I = 0.01\text{ M NaCl}$ .

with the m-NPs/GO ratio increasing from 0:1 to 100:1. Thus, the promotion effects followed the order montmorillonite > ZnO > kaolin >  $\text{Fe}_2\text{O}_3$ . Unlike the present research results, kaolin and montmorillonite only restrained the adsorption of 17 $\beta$ -estradiol (E2) and bisphenol A (BPA) on GO or reduced graphene oxide (rGO) (Sun et al., 2017). Moreover, the results were also different from the studies of E2 adsorption on CNTs in the existence of ZnO and  $\text{Fe}_2\text{O}_3$ , E2 adsorption capacities increased markedly with the increase of  $\text{Fe}_2\text{O}_3/\text{CNTs}$  ratio, but decreased slightly with the increasing of ZnO/CNTs ratio (Shi et al., 2017). This might be attributed to the different reaction characteristics between m-NPs and adsorbates or adsorbents and adsorbates.

To further investigate the promotion effects, the removal efficiencies of TC by GO and m-NPs in the absence and existence of 0.005 g GO were determined. From Fig. S1, TC removal efficiency by GO is about 18% at  $\text{pH} = 7$  and the removal capacity of TC by four kinds of m-NPs all show a significant increase with increasing the mass of m-NPs. The adsorption capacity by m-NPs alone also followed the order montmorillonite > ZnO > kaolin >  $\text{Fe}_2\text{O}_3$ , demonstrating that TC could be adsorbed on the m-NPs surface, especially at higher concentrations of m-NPs. In the synergistic system of GO and m-NPs, TC removal efficiency was higher than that of GO and m-NPs alone, and the adsorption was not equal to the sum of the two. The enhanced adsorption

**Table 3**

Adsorption isotherm parameters of TC on GO in the existence of m-NPs.

Adsorbents		Langmuir					Freundlich				
		$q_m$ (mg/g)	$K_L$ (L/mg)	$R^2$	RMSE	$\chi^2$	$K_f [(mg/g)/(mg/L)^N]$	N	$R^2$	RMSE	$\chi^2$
$\text{Fe}_2\text{O}_3/\text{GO}$	0:1	1066.55	$7.64 \times 10^{-4}$	0.993	4.42	19.53	1.33	0.88	0.997	2.98	8.89
	10:1	101.09	0.014	0.887	5.37	28.80	8.98	0.40	0.971	2.74	7.48
	50:1	210.51	0.013	0.871	12.41	154.06	16.54	0.42	0.973	5.67	32.10
	100:1	190.76	0.053	0.838	10.49	110.05	56.82	0.22	0.985	3.21	10.29
ZnO/GO	0:1	1066.55	$7.64 \times 10^{-4}$	0.993	4.42	19.53	1.33	0.88	0.997	2.98	8.89
	10:1	2141.79	0.030	0.978	52.04	2708.28	105.53	0.66	0.990	35.29	1245.64
	50:1	2127.42	0.039	0.983	45.95	2111.64	132.00	0.64	0.990	36.56	1336.36
	100:1	1729.35	0.087	0.915	105.21	11,069.79	255.67	0.48	0.956	75.79	5744.52
Montmorillonite/GO	0:1	1066.55	$7.64 \times 10^{-4}$	0.993	4.42	19.53	1.33	0.88	0.997	2.98	8.89
	10:1	1750.71	0.250	0.859	141.09	19,905.95	458.16	0.44	0.925	102.63	10,532.78
	50:1	1816.79	0.413	0.952	86.31	7449.05	539.90	0.53	0.986	46.31	2144.95
	100:1	3779.95	0.375	0.936	109.19	11,921.50	1012.54	0.72	0.949	97.49	9503.87
Kaolin/GO	0:1	1066.55	$7.64 \times 10^{-4}$	0.993	4.42	19.53	1.33	0.88	0.997	2.98	8.89
	10:1	177.83	0.022	0.799	13.08	171.21	25.12	0.33	0.934	7.48	56.02
	50:1	602.10	0.019	0.912	35.70	1274.48	50.35	0.44	0.990	11.73	137.69
	100:1	652.00	0.130	0.787	80.28	6445.08	187.56	0.27	0.994	12.98	168.39

capability was attributed to the possible enhancing performance of GO induced by m-NPs. However, the different degrees of promotion effect shown by the four m-NPs might be ascribed to their different surface characteristics, such as large specific surface area and pore volume, as well as the surface charge.

Therefore, the adsorption of TC onto m-NPs led to the increase of TC adsorption in the binary system of GO and m-NPs. However, the inhibitory effects of 10:1 Fe<sub>2</sub>O<sub>3</sub>/GO on TC adsorption might be caused by the slight blocking of the adsorption sites on the surface of GO, and the blockage effect could be greater than the adsorption effect in a small amount of Fe<sub>2</sub>O<sub>3</sub>.

1/N is the parameter associated with the intensity of adsorption or surface heterogeneity of the material. Generally, the value of  $1/N < 1$  verifies a normal Freundlich isotherm, becoming more and more heterogeneous as it tends to zero, while  $1/N > 1$  implies synergistic adsorption (Fytianos et al., 2000). In this study, all 1/N values obtained from TC adsorption were  $>1$ , suggesting that the adsorption process involved a cooperative adsorption by GO and m-NPs.

### 3.4. Effect of pH

The influence of pH is displayed in Fig. 5. In homogeneous system of GO, the TC adsorption capacity decreased as increasing pH. After the addition of montmorillonite, ZnO and kaolin, TC adsorption capacity first increased and then decreased with pH from 3.0 to 11.0. The addition of Fe<sub>2</sub>O<sub>3</sub> showed a downward trend in the TC adsorption on GO by varying the pH from 3.0 to 11.0 (Fig. 5). In heterogeneous system of GO and m-NPs, the adsorption capacities of TC were obviously enhanced than in homogeneous system of GO at various pH values. This pH-dependent adsorption could be traceable to the distribution of TC species and the surface charges of m-NPs and GO in aquatic solution.

TC has three acid dissociation constants ( $pK_a = 3.3, 7.7, \text{ and } 9.7$ ) and exists as a cationic (TCH<sup>3+</sup>), zwitterionic (TCH<sub>2</sub><sup>0</sup>), and anionic (TCH<sup>-</sup> or TC<sup>2-</sup>) species, respectively (Gao et al., 2012). The surface charges of m-NPs, GO, m-NPs/GO are measured by zeta potentials measurement and shown in Fig. S2. GO was negatively charged under varying pH from 3.0 to 11.0 due to rich oxygen-containing functional groups on its surface, which was conducive to the adsorption of TCH<sup>3+</sup> and TCH<sub>2</sub><sup>0</sup>. However, with increasing pH value, the adsorption amount of TC gradually decreased because the increase of pH value promoted the deprotonation of the oxygen-containing groups on TC molecule and GO. The electron-acceptor ability of these parts was weakened with the increasing of pH value, inhibiting the binding of cation- $\pi$  and  $\pi$ - $\pi$  bonds with GO (Gao et al., 2012). Under the alkaline conditions, the adsorption capacity of TC decreased with increasing pH due to the electrostatic repulsion between negatively charged TC and m-NPs/GO, whereas TC adsorption showed different results by adding various m-NPs under the acidic conditions. The addition of the negatively charged kaolin enhanced the negative charge onto the surface of GO. In the presence of kaolin, TC adsorption amount started to slightly increase with increasing pH value to 7 because of the mutual attractive interactions between positively charged TC and negatively charged kaolin/GO. Montmorillonite had obviously promotion effect on TC adsorption on GO over the tested pH range, but there is little difference in adsorption capacity under different pH values. In the mixed system of GO and ZnO, adsorption ability of TC was enhanced in the pH value from 3.0 to 7.0, which might be related to the salting out effect of Zn<sup>2+</sup> under acidic conditions. ZnO was unstable in solution and approximately 100% Zn<sup>2+</sup> was readily transferred into aqueous solution under acidic conditions. The release of Zn<sup>2+</sup> could improve the activity coefficient of TC, reduced the solubility of TC, and hence promoted the adsorption of TC on GO (i.e. salting-out effect). Besides, electrostatic interaction might also play a key role in

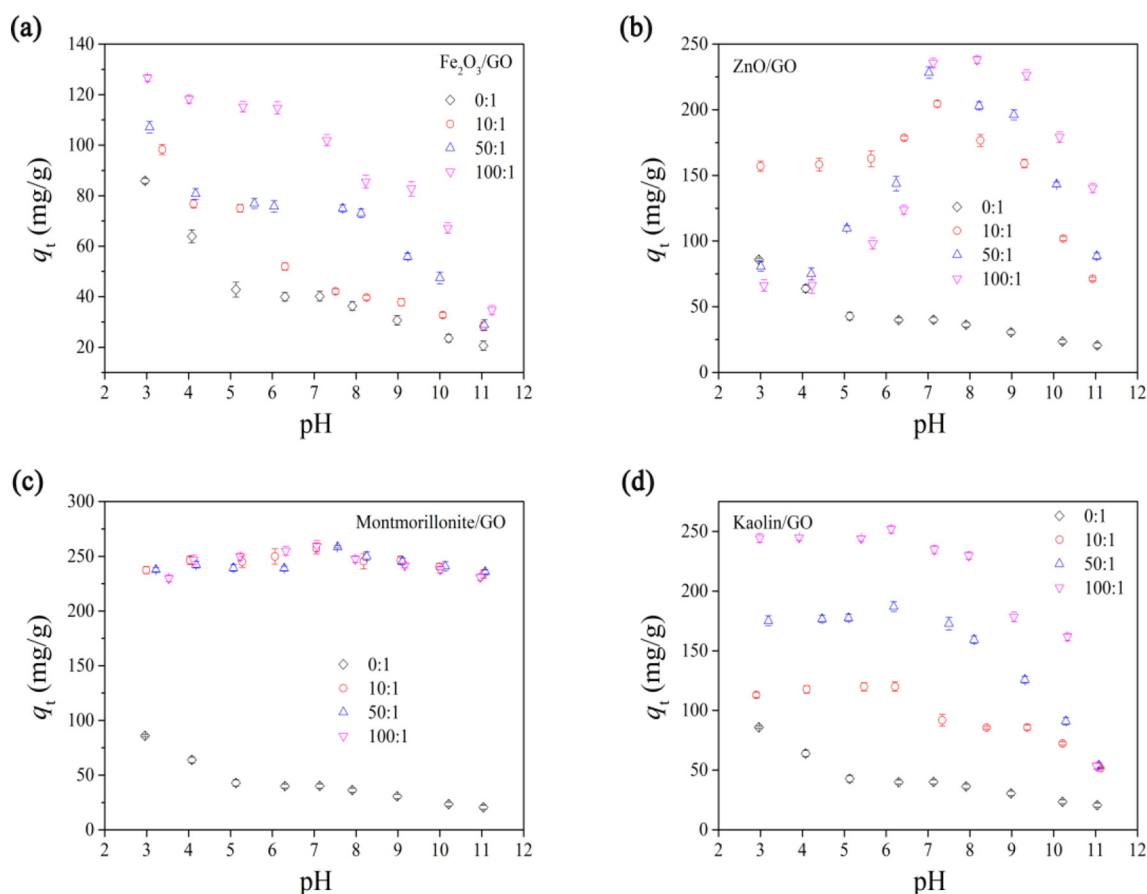


Fig. 5. pH effect on TC adsorption by GO under different m-NPs/GO ratios.  $C_{0(TC)} = 50 \text{ mg/L}$ ,  $T = 25 \text{ }^\circ\text{C}$ ,  $I = 0.01 \text{ M NaCl}$ .

acidic conditions owing to the more negative charge of ZnO/GO was more beneficial to positively charged TC adsorption at  $\text{pH} < 7$  and the more positive charge of ZnO/GO was more beneficial to negatively charged TC adsorption at  $\text{pH} 7\text{--}10$ . The addition of  $\text{Fe}_2\text{O}_3$  led to a significant decrease in TC uptake on GO. The effect of high concentration  $\text{Fe}_2\text{O}_3$  ( $\text{Fe}_2\text{O}_3/\text{GO} \geq 50:1$ ) was ascribed to the electrostatic repulsion between positively charged TC and  $\text{Fe}_2\text{O}_3/\text{GO}$  at  $\text{pH} < 7$ . Besides, the heteroaggregation between the positive charges of  $\text{Fe}_2\text{O}_3$  and negatively charged GO might reduce some adsorption sites. When the  $\text{Fe}_2\text{O}_3/\text{GO}$  ratio was 10:1, the heteroaggregation might be the major factor for the decrease of adsorption capacity at  $\text{pH} < 7$ . Shi et al. (Shi et al., 2017) identified the effects of  $\text{Fe}_2\text{O}_3$  on the uptake of E2 by carbon nanotubes. Likewise, the electrostatic attraction between negatively charged

CNTs and positively charged  $\text{Fe}_2\text{O}_3$  promoted the heteroaggregation at  $\text{pH} < \text{pH}_{\text{zpc}}$ . The influence mechanisms of m-NPs on TC adsorption on GO were further proved by TEM and DLVO analysis.

### 3.5. Comparison to other adsorbents

The effect of four m-NPs (montmorillonite, ZnO, kaolin and  $\text{Fe}_2\text{O}_3$ ) on the adsorption of TC by different adsorbents are investigated at initial TC concentration of 50 mg/L and exhibited in Fig. 6. As reflected by Fig. 6, all m-NPs show promoting effect on TC adsorption by GO, BC, MWCNT, PAC and GAC with increasing m-NPs concentration resulting from the adsorption of TC to m-NPs. Compared with the influence of m-NPs on the adsorption of TC by other four adsorbents, the m-NPs

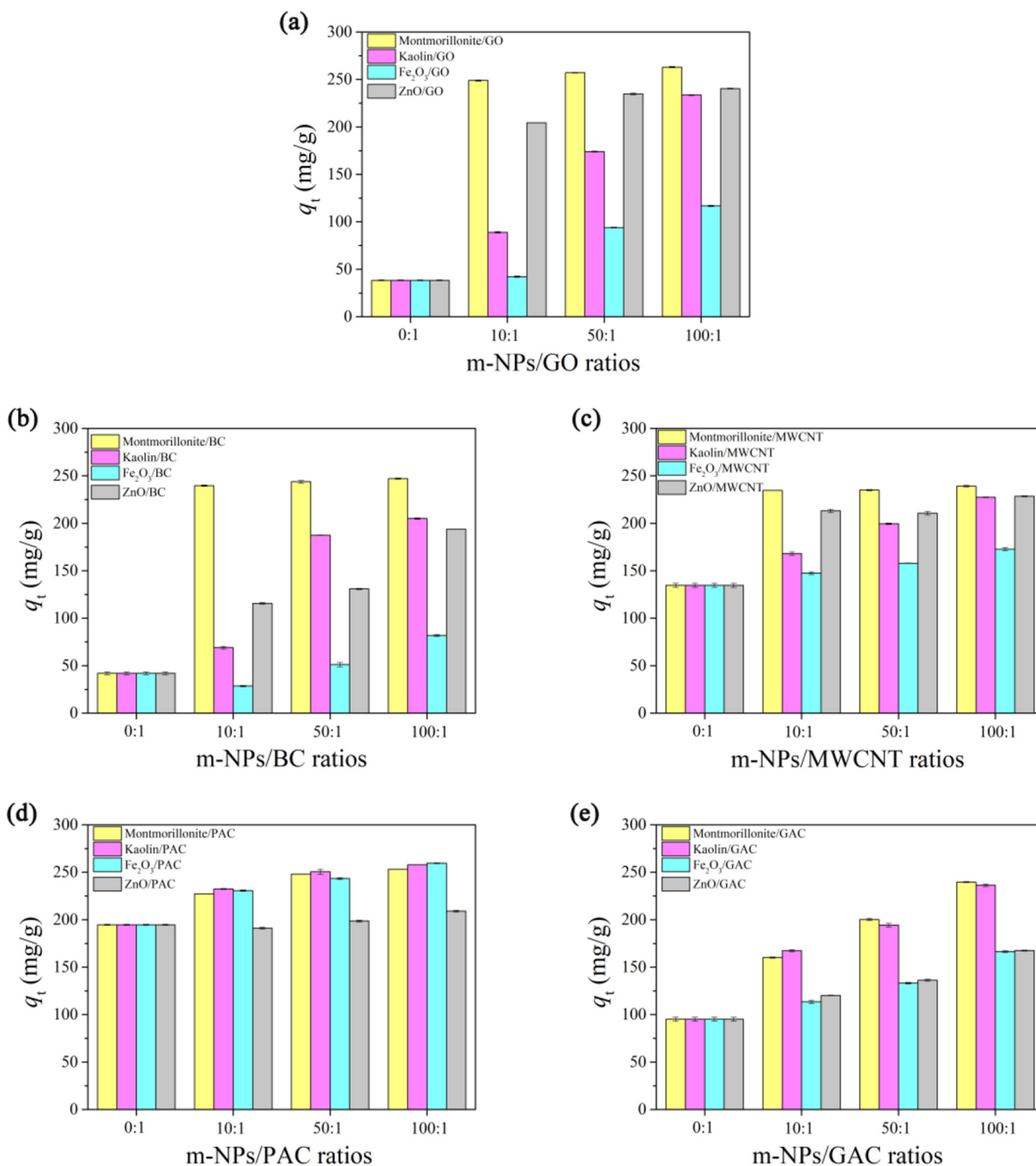
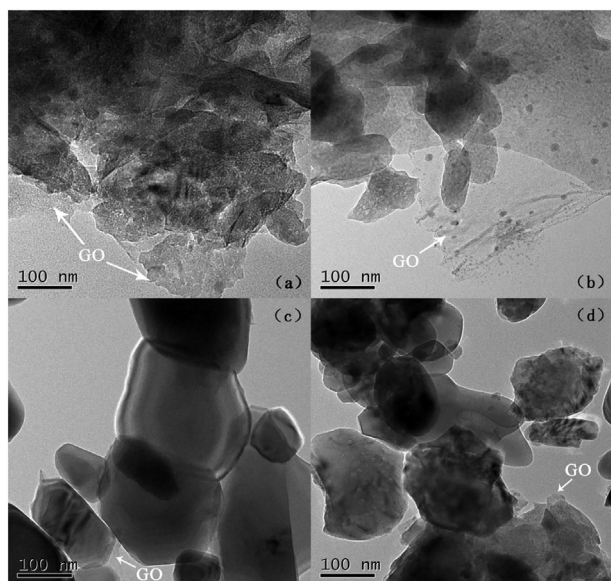


Fig. 6. Different adsorbents for TC adsorption at different m-NPs/adsorbents ratios.  $C_{0(\text{TC})} = 50 \text{ mg/L}$ ,  $T = 25 \text{ }^\circ\text{C}$ ,  $I = 0.01 \text{ M NaCl}$ .



**Fig. 7.** (a)–(d) are the TEM images of montmorillonite/GO, kaolin/GO, ZnO/GO and Fe<sub>2</sub>O<sub>3</sub>/GO, respectively.

presented the greatest promoting efficiency for TC adsorption on GO. It was indicated that the combined effect of GO and m-NPs was the best among the five adsorbents for 50 mg/L TC removal.

### 3.6. Influencing mechanisms of m-NPs

The surface morphology of the m-NPs/GO heteroaggregates were observed using TEM (Fig. 7). From TEM images, the exterior surface of GO is attached by stonelike or platelike m-NPs, resulting in the blockage of the adsorption sites on GO surface or increase the aggregation of GO sheets. However, only limited adsorption sites on GO surface were blocked by m-NPs owing to their smaller surface area, and these m-NPs particles could increase the adsorption sites for TC adsorption due to either the synergistic effect of m-NPs and GO or the adsorption effect of m-NPs/GO heteroaggregation. Similar research results have been reported by Shi et al. (Shi et al., 2017), demonstrating that the E2 adsorption on CNTs was notably improved with the addition of Fe<sub>2</sub>O<sub>3</sub>. In the binary system of montmorillonite/GO and kaolin/GO (Fig. 7a and b), the TEM images show some partially overlapped transparent films on

the edge of montmorillonite/GO and kaolin/GO, indicating that GO tends to homoaggregate, whereas montmorillonite or kaolin is prone to heteroaggregate with GO. Hence, GO first homoaggregated, and then smaller montmorillonite or kaolin particles entered these porous aggregates. However, in the present of ZnO (Fig. 7c), the heteroaggregation between GO and ZnO was superior to the homoaggregation between the same type of m-NPs or GO. These results were consistent with the theoretical calculations of DLVO. Compared with the TEM images of ZnO/GO heteroaggregates (Fig. 7c), more wrinkles appeared on the surface of Fe<sub>2</sub>O<sub>3</sub>/GO heteroaggregates (Fig. 7d), which were probably dependent on Fe<sub>2</sub>O<sub>3</sub> first homoaggregation and then heteroaggregate with GO.

### 3.7. DLVO theoretical analysis

The measured contact angles and calculated Hamaker constants used for DLVO theory analysis are presented in Table S1. The DLVO interactions between GO/GO, m-NPs/m-NPs, m-NPs/GO particles are exhibited in Fig. 8. In the homogeneous system, the maximum energy barrier between GO/GO ( $9.40 \times 10^{-20}$  J) was weaker than those of between kaolin/kaolin ( $2.55 \times 10^{-18}$  J) and montmorillonite/montmorillonite ( $3.05 \times 10^{-19}$  J), demonstrating preferable aggregation of GO than that of kaolin and montmorillonite. In binary systems of kaolin and GO, the maximum repulsive energy between GO and kaolin ( $5.13 \times 10^{-19}$  J) were markedly lower than those between pairs of kaolin ( $2.55 \times 10^{-18}$  J) but greater than those between pairs of GO ( $9.40 \times 10^{-20}$  J). Hence, in heterogeneous systems of kaolin/GO, GO was likely to homoaggregate between identical particles, while kaolin particles were inclined to heteroaggregate with GO rather than to homoaggregate. The electrostatic repulsion existed between the same charged GO/GO and kaolin/kaolin, whereas relatively lower degree of electrostatic repulsion between pairs of GO was beneficial to their homoaggregation. Thus, in the mix system of GO and kaolin, GO was prone to be homopolymerized first, and then heteropolymerized with kaolin. Similar results also existed in binary systems of GO and montmorillonite. In the homogeneous system of ZnO, the positive  $\Phi_{\text{tot}}$  suggested the existence of electrostatic repulsion between ZnO/ZnO. However, in the hybrid systems of ZnO/GO, the negative  $\Phi_{\text{tot}}$  confirmed strong attraction between oppositely charged GO and ZnO, which promoted the heteroaggregation rather than the homoaggregation. For Fe<sub>2</sub>O<sub>3</sub>, the maximum energy barrier between pairs of GO particles ( $9.40 \times 10^{-20}$  J) was much higher than those between pairs of Fe<sub>2</sub>O<sub>3</sub>/GO ( $1.04 \times 10^{-20}$  J) and Fe<sub>2</sub>O<sub>3</sub>/Fe<sub>2</sub>O<sub>3</sub> ( $1.47 \times 10^{-22}$  J), whereas the maximum energy barrier of Fe<sub>2</sub>O<sub>3</sub>/Fe<sub>2</sub>O<sub>3</sub> was much lower than Fe<sub>2</sub>O<sub>3</sub>/GO,

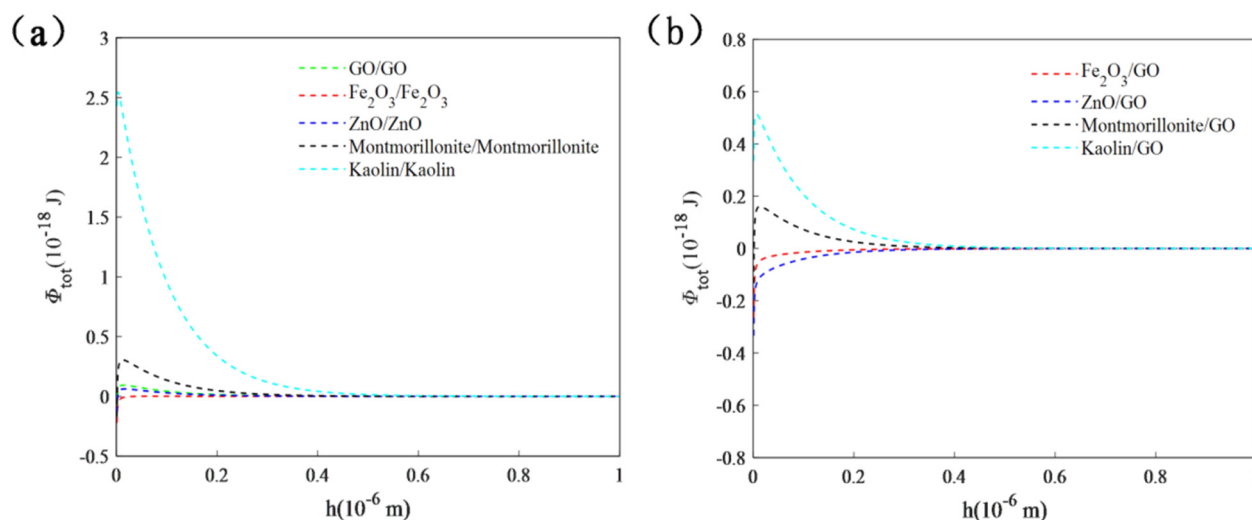


**Fig. 8.** Interaction energies between GO/GO, m-NPs/m-NPs and m-NPs/GO versus separation distance calculated by DLVO theory. m-NPs/GO = 10:1,  $T = 25$  °C,  $\text{pH} = 7.0$ ,  $I = 0.01$  mol/L NaCl.

demonstrating that Fe<sub>2</sub>O<sub>3</sub> was prone to first homoaggregate and then heteroaggregate with GO in the mix system of GO and Fe<sub>2</sub>O<sub>3</sub>.

#### 4. Conclusions

The findings of this study investigated the adsorption characteristics of TC by GO with presence of m-NPs (Fe<sub>2</sub>O<sub>3</sub>, ZnO, montmorillonite and kaolin). Results showed that adsorption kinetics was better fitted by pseudo-second-order kinetic model than the first-order kinetic model, which was controlled by both film and intraparticle diffusion processes. The adsorption equilibrium time of TC to GO increased with increase of m-NPs/GO ratios. The presence of different amounts of m-NPs enhanced the TC adsorption capacity except for that at Fe<sub>2</sub>O<sub>3</sub>/GO = 10:1 and the adsorption capacity significantly increased with increasing TC concentration. The promotion effects could be ascribed to the adsorption of TC onto m-NPs, whereas the inhibitory effects of 10:1 Fe<sub>2</sub>O<sub>3</sub>/GO might be attributed to the blockage effect greater than the adsorption effect in a small amount of Fe<sub>2</sub>O<sub>3</sub>. In addition, the experimental data clearly showed that the introduction of m-NPs contributed to an increase of TC adsorption on GO in the tested pH range. By comparing the effects of m-NPs on the adsorption of TC on five adsorbents (GO, BC, MWCNT, PAC and GAC), it confirmed that the combined action of GO and m-NPs has the greatest promotion efficiency for TC removal. According to TEM images and DLVO calculation, GO was more inclined to first homoaggregate and then heteroaggregate with montmorillonite and kaolin in the composite system. However, Fe<sub>2</sub>O<sub>3</sub> was first homoaggregate and then heteroaggregate with GO, and the electrostatic attraction between oppositely charged GO and ZnO favored their heteroaggregation in the binary system of GO and ZnO.

#### Declaration of competing interest

The authors declare that they have no known competing financial interests or personal relationships that could have appeared to influence the work reported in this paper.

#### Acknowledgments

This research was financially supported by the National Natural Science Foundation of China (Grants Nos. 51521006, 51609268, and 51809019), Natural Science Foundation of Hunan Province, China (grants 2018JJ3096), Open Fund of Guangdong Provincial Key Laboratory of Petrochemical Pollution Process and Control, Guangdong University of Petrochemical Technology (No. 2018B030322017).

#### Appendix A. Supplementary data

Supplementary data to this article can be found online at <https://doi.org/10.1016/j.scitotenv.2020.137283>.

#### References

- Abdelrahman, E.A., Hegazey, R.M., Kotp, Y.H., Ahmed, A., 2019. Facile synthesis of Fe<sub>2</sub>O<sub>3</sub> nanoparticles from Egyptian insecticide cans for efficient photocatalytic degradation of methylene blue and crystal violet dyes. *Spectrochim. Acta A* 222, 117195.
- Andre, N., Tian, X., Lutz, M.D., Ning, L., 2006. Toxic potential of materials at the nanolevel. *Science* 311 (5761), 622–627.
- Asfaram, A., Ghaedi, M., Hajati, S., Goudarzi, A., 2016. Synthesis of magnetic gamma-Fe<sub>2</sub>O<sub>3</sub>-based nanomaterial for ultrasonic assisted dyes adsorption: modeling and optimization. *Ultrason. Sonochem.* 32, 418–431.
- Awad, A.M., Shaikh, S.M.R., Jalab, R., Gulied, M.H., Nasser, M.S., Benamor, A., Adham, S., 2019. Adsorption of organic pollutants by natural and modified clays: a comprehensive review. *Sep. Purif. Technol.* 228, 115719.
- Bhatt, I., Tripathi, B.N., 2011. Interaction of engineered nanoparticles with various components of the environment and possible strategies for their risk assessment. *Chemosphere* 82 (3), 308–317.
- Chen, B., Sun, W., Wang, C., Guo, X., 2017. Size-dependent impact of inorganic nanoparticles on sulfamethoxazole adsorption by carbon nanotubes. *Chem. Eng. J.* 316, 160–170.
- Chen, H., Gao, B., Li, H., 2015. Removal of sulfamethoxazole and ciprofloxacin from aqueous solutions by graphene oxide. *J. Hazard. Mater.* 282, 201–207.
- Chen, Z., Zhang, N., Xu, Y.-J., 2013. Synthesis of graphene-ZnO nanorod nanocomposites with improved photoactivity and anti-photocorrosion. *CrystEngComm* 15 (15), 3022.
- Duan, Q., Li, X., Wu, Z., Alsaedi, A., Hayat, T., Chen, C., Li, J., 2019. Adsorption of 17β-estradiol from aqueous solutions by a novel hierarchically nitrogen-doped porous carbon. *J. Colloid Interface Sci.* 533, 700–708.
- Fytianos, K., Voudrias, E., Kokkalis, E., 2000. Sorption-desorption behaviour of 2,4-dichlorophenol by marine sediments. *Chemosphere* 40 (1), 3–6.
- Gao, Y., Li, Y., Zhang, L., Huang, H., Hu, J., Shah, S.M., Su, X., 2012. Adsorption and removal of tetracycline antibiotics from aqueous solution by graphene oxide. *J. Colloid Interface Sci.* 368 (1), 540–546.
- Geng, Y., Wang, S.J., Kim, J.K., 2009. Preparation of graphite nanoplatelets and graphene sheets. *J. Colloid Interface Sci.* 336 (2), 592–598.
- Ghadim, E.E., Manouchehri, F., Soleimani, G., Hosseini, H., Kimiagar, S., Nafisi, S., 2013. Adsorption properties of tetracycline onto graphene oxide: equilibrium, kinetic and thermodynamic studies. *PLoS One* 8, 1–9.
- Ghaedi, M., Ansari, A., Habibi, M.H., Asghari, A.R., 2014. Removal of malachite green from aqueous solution by zinc oxide nanoparticle loaded on activated carbon: kinetics and isotherm study. *J. Ind. Eng. Chem.* 20 (1), 17–28.
- Hu, X., Liu, Y., Wang, H., Zeng, G., Hu, X., Guo, Y., Li, T., Chen, A., Jiang, L., Guo, F., 2015. Adsorption of copper by magnetic graphene oxide-supported β-cyclodextrin: effects of pH, ionic strength, background electrolytes, and citric acid. *Chem. Eng. Res. Des.* 93, 675–683.
- Ji, Z., Pei, Y., 2019. Bibliographic and visualized analysis of geopolymer research and its application in heavy metal immobilization: a review. *J. Environ. Manag.* 231, 256–267.
- Jiang, L., Liu, Y., Zeng, G., Liu, S., Hu, X., Zhou, L., Tan, X., Liu, N., Li, M., Wen, J., 2018a. Adsorption of estrogen contaminants (17β-estradiol and 17α-ethynylestradiol) by graphene nanosheets from water: effects of graphene characteristics and solution chemistry. *Chem. Eng. J.* 339, 296–302.
- Jiang, L., Liu, Y., Zeng, G., Liu, S., Que, W., Li, J., Li, M., Wen, J., 2018b. Adsorption of 17β-estradiol by graphene oxide: effect of heteroaggregation with inorganic nanoparticles. *Chem. Eng. J.* 343, 371–378.
- Kenawy, I.M.M., Eldefrawy, M.M., Eltabey, R.M., Zaki, E.G., 2019. Melamine grafted chitosan-montmorillonite nanocomposite for ferric ions adsorption: central composite design optimization study. *J. Clean. Prod.* 241, 118189.
- Ki-Tae, K., Edgington, A.J., Klaine, S.J., Jae-Weon, C., Sang, D., Kim, 2009. Influence of multiwalled carbon nanotubes dispersed in natural organic matter on speciation and bioavailability of copper. *Environ. Sci. Technol.* 43 (23), 8979–8984.
- Li, M.F., Liu, Y.G., Zeng, G.M., Liu, S.B., Hu, X.J., Shu, D., Jiang, L.H., Tan, X.F., Cai, X.X., Yan, Z.L., 2017b. Tetracycline adsorbed onto nitrilotriacetic acid-functionalized magnetic graphene oxide: influencing factors and uptake mechanism. *J. Colloid Interface Sci.* 485, 269–279.
- Li, M.F., Liu, Y.G., Zeng, G.M., Liu, N., Liu, S.B., 2019. Graphene and graphene-based nanocomposites used for antibiotics removal in water treatment: a review. *Chemosphere* 226, 360–380.
- Li, M., Liu, Y., Liu, S., Shu, D., Zeng, G., Hu, X., Tan, X., Jiang, L., Yan, Z., Cai, X., 2017a. Cu(II)-influenced adsorption of ciprofloxacin from aqueous solutions by magnetic graphene oxide/nitrilotriacetic acid nanocomposite: competition and enhancement mechanisms. *Chem. Eng. J.* 319, 219–228.
- Lin, Y., Xu, S., Li, J., 2013. Fast and highly efficient tetracyclines removal from environmental waters by graphene oxide functionalized magnetic particles. *Chem. Eng. J.* 225, 679–685.
- Liu, F.F., Zhao, J., Wang, S., Xing, B., 2016. Adsorption of sulfonamides on reduced graphene oxides as affected by pH and dissolved organic matter. *Environ. Pollut.* 210, 85–93.
- Liu, S., Liu, Y., Jiang, L., Zeng, G., Li, Y., Zeng, Z., Wang, X., Ning, Q., 2019a. Removal of 17β-estradiol from water by adsorption onto montmorillonite-carbon hybrids derived from pyrolysis carbonization of carboxymethyl cellulose. *J. Environ. Manag.* 236, 25–33.
- Liu, Z., Rios-Carvajal, T., Andersson, M.P., Ceccato, M., Stipp, S.L.S., Hassenkam, T., 2019b. Ion effects on molecular interaction between graphene oxide and organic molecules. *Environ. Sci. Nano* 6 (7), 2281–2291.
- Olusegun, S.J., de Sousa Lima, L.F., Mohalleh, N.D.S., 2018. Enhancement of adsorption capacity of clay through spray drying and surface modification process for wastewater treatment. *Chem. Eng. J.* 334, 1719–1728.
- Rashidi Nodeh, H., Sereshti, H., 2016. Synthesis of magnetic graphene oxide doped with strontium titanium trioxide nanoparticles as a nanocomposite for the removal of antibiotics from aqueous media. *RSC Adv.* 6 (92), 89953–89965.
- Razmi, F.A., Ngadi, N., Wong, S., Inuwa, I.M., Opotu, L.A., 2019. Kinetics, thermodynamics, isotherm and regeneration analysis of chitosan modified pandan adsorbent. *J. Clean. Prod.* 231, 98–109.
- Shaban, M., Hassouna, M.E.M., Nasief, F.M., AbuKhadra, M.R., 2017. Adsorption properties of kaolinite-based nanocomposites for Fe and Mn pollutants from aqueous solutions and raw ground water: kinetics and equilibrium studies. *Environ. Sci. Pollut. Res. Int.* 24 (29), 22954–22966.
- Shi, W., Li, S., Chen, B., Wang, C., Sun, W., 2017. Effects of Fe<sub>2</sub>O<sub>3</sub> and ZnO nanoparticles on 17β-estradiol adsorption to carbon nanotubes. *Chem. Eng. J.* 326, 1134–1144.
- Sun, W., Zhang, C., Xu, N., Ni, J., 2015. Effect of inorganic nanoparticles on 17β-estradiol and 17α-ethynylestradiol adsorption by multi-walled carbon nanotubes. *Environ. Pollut.* 205, 111–120.
- Sun, W., Wang, C., Pan, W., Li, S., Chen, B., 2017. Effects of natural minerals on the adsorption of 17β-estradiol and bisphenol A on graphene oxide and reduced graphene oxide. *Environ. Sci. Nano* 4 (6), 1377–1388.
- Wang, H., Yuan, X., Wu, Y., Huang, H., Peng, X., Zeng, G., Zhong, H., Liang, J., Ren, M., 2013. Graphene-based materials: fabrication, characterization and application for the de-

- contamination of wastewater and waste gas and hydrogen storage/generation. *Adv. Colloid Interf. Sci.* 195–196, 19–40.
- Wang, J., Chen, Z., Chen, B., 2014. Adsorption of polycyclic aromatic hydrocarbons by graphene and graphene oxide nanosheets. *Environ. Sci. Technol.* 48 (9), 4817–4825.
- Yang, S.T., Chang, Y., Wang, H., Liu, G., Chen, S., Wang, Y., Liu, Y., Cao, A., 2010. Folding/aggregation of graphene oxide and its application in  $\text{Cu}^{2+}$  removal. *J. Colloid Interface Sci.* 351 (1), 122–127.
- Yao, Y., Miao, S., Liu, S., Ma, L.P., Sun, H., Wang, S., 2012. Synthesis, characterization, and adsorption properties of magnetic  $\text{Fe}_3\text{O}_4$ @graphene nanocomposite. *Chem. Eng. J.* 184, 326–332.
- Yin, Z., Liu, Y., Liu, S., Jiang, L., Tan, X., Zeng, G., Li, M., Liu, S., Tian, S., Fang, Y., 2018. Activated magnetic biochar by one-step synthesis: enhanced adsorption and coadsorption for 17 $\beta$ -estradiol and copper. *Sci. Total Environ.* 639, 1530–1542.
- Yu, F., Li, Y., Han, S., Ma, J., 2016. Adsorptive removal of antibiotics from aqueous solution using carbon materials. *Chemosphere* 153, 365–385.
- Yusuf, M., Elfghi, F.M., Zaidi, S.A., Abdullah, E.C., Khan, M.A., 2015. Applications of graphene and its derivatives as an adsorbent for heavy metal and dye removal: a systematic and comprehensive overview. *RSC Adv.* 5 (62), 50392–50420.
- Zhang, L., Song, X., Liu, X., Yang, L., Pan, F., Lv, J., 2011. Studies on the removal of tetracycline by multi-walled carbon nanotubes. *Chem. Eng. J.* 178, 26–33.
- Zhang, Q., Zhao, D., Ding, Y., Chen, Y., Li, F., Alsaedi, A., Hayat, T., Chen, C., 2019. Synthesis of Fe–Ni/graphene oxide composite and its highly efficient removal of uranium(VI) from aqueous solution. *J. Clean. Prod.* 230, 1305–1315.
- Zhou, Y., Apul, O.G., Karanfil, T., 2015. Adsorption of halogenated aliphatic contaminants by graphene nanomaterials. *Water Res.* 79, 57–67.
- Zhou, Y., Liu, X., Xiang, Y., Wang, P., Zhang, J., Zhang, F., Wei, J., Luo, L., Lei, M., Tang, L., 2017. Modification of biochar derived from sawdust and its application in removal of tetracycline and copper from aqueous solution: adsorption mechanism and modelling. *Bioresour. Technol.* 245, 266–273.
- Zhu, C., Yang, W.L., He, H., Yang, C., Yu, J., Wu, X., Zeng, G., Tarre, S., Green, M., 2018. Preparation, performances and mechanisms of magnetic *Saccharomyces cerevisiae* bionanocomposites for atrazine removal. *Chemosphere* 200, 380–387.